(Received 20 May 2025, Accepted 25 July 2025, Scheduled 5 August 2025)

Single-Port Microwave Sensor Using Defected Ground Structure Complementary Split Ring Resonator for Solid Material Characterization

Rayan A. Ba Amer[1], Noor Azwan Shairi[1,*], Maizatul Alice Meor Said[1], Zahriladha Zakaria[1], Mohamad Harris Misran[1], Adib Bin Othman[1], Syah Alam[2], and Sharul Kamal Abdul Rahim[3]

[1]*Microwave Research Group, Centre for Telecommunication Research and Innovation (CeTRI) Fakulti Teknologi dan Kejuruteraan Elektronik dan Komputer (FTKEK) Universiti Teknikal Malaysia Melaka (UTeM), Melaka, Malaysia*
[2]*Department of Electrical Engineering, Universitas Trisakti, Jakarta, Indonesia*
[3]*Faculty of Electrical Engineering, Universiti Teknologi Malaysia, Johor, Malaysia*

ABSTRACT: This paper proposes a single-port microwave sensor for solid material characterization, based on defected ground structures (DGSs) with complementary split-ring resonators (CSRRs). Fabricated on an RO5880 substrate, the sensor was analyzed through both simulation and experimental measurement. Electromagnetic simulation and optimization were conducted using CST Studio Suite within the 1.5–3.0 GHz frequency range. The sensor's performance was evaluated with three materials of known permittivity: RO5880, RO4350, and FR-4. Results show that the two proposed configurations, one with a DGS CSRR (Design A) and the other with an added slot on the DGS CSRR (Design B) yielding Q-factors of 332 and 357, respectively. The higher Q-factor in Design B indicates increased sensitivity across all tested materials compared to Design A. For example, Design B achieved the highest sensitivity of 4.71% for RO5880 material compared to Design A. Thus, the added slot enhanced field coupling, improving measurement sensitivity and confirming the sensor's suitability for microwave-based solid material characterization.

1. INTRODUCTION

Recent advancements in planar microwave sensor technology have broadened their application in material characterization. These sensors are now used in areas such as food quality monitoring, pharmaceutical analysis, and non-destructive testing [1]. They enable accurate extraction of electromagnetic properties like permittivity and permeability. Such properties are crucial for developing high-frequency circuits and conducting material research [2, 3]. Conventional methods like waveguides offer high precision but are often bulky, costly, and require large sample volumes [4, 5]. To address these limitations, planar resonator-based sensors have emerged as promising alternatives due to their compactness, low cost, and ease of integration. However, their limited Q-factor and sensitivity restrict their applicability in demanding measurement scenarios [6].

Defected ground structure (DGS) has been widely applied in both active and passive microwave devices, including filters [7–9], antennas [10–12], switches [13, 14], and amplifiers [15] to improve parameters such as spurious or harmonics suppression, isolation, mutual coupling, improve impedance matching, and size reduction. In recent years, the integration of DGS into planar microwave sensors has attracted growing interest in the field of microwave sensor design [16–20]. The use of DGS in microwave sensor enhances electric field confinement around the sensing region, increasing sensitivity to changes in the dielectric properties of nearby materials [21]. Variations in the permittivity of the material under test result in measurable shifts in the resonator's frequency response, enabling DGS-based microwave sensors to detect physical parameters such as solid and liquid contents [22].

On the other hand, split ring resonator (SRR) is a compact resonant structure designed to confine electromagnetic fields effectively [23–25]. This confinement makes SRRs suitable for high-sensitivity dielectric sensing. Comprising concentric metallic rings with splits, SRRs resonate when being exposed to electromagnetic waves, and any variation in the surrounding material's permittivity causes measurable shifts in resonant frequency [26–28]. Their performance can be tuned through geometric parameters such as ring spacing and split position, while enhancements like complementary SRRs (CSRRs) [29–31] and spur lines [32] can improve field interaction and sensitivity. SRRs have been widely applied in applications ranging from biosensing and fluid detection to solid material characterization and analysis.

Recent work has combined structures like DGS with SRR or CSRR to improve resonance behavior and field confinement [20–22]. This integration aims to enhance material characterization by increasing sensitivity to permittivity changes [33–35]. However, these microwave sensors are predominantly configured in a two-port design, rather than a single-port structure. The potential advantages of single-port

* Corresponding author: Noor Azwan Shairi (noorazwan@utem.edu.my).

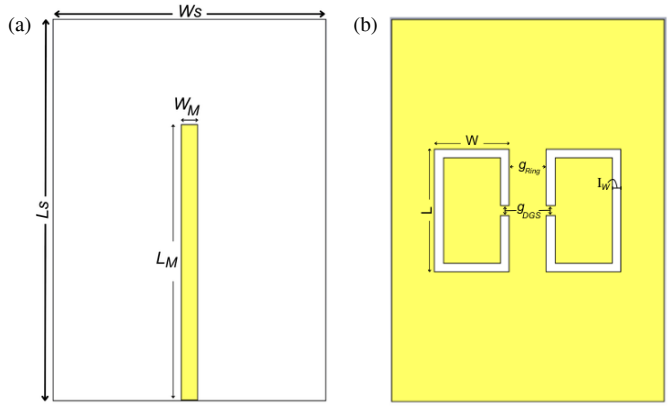

FIGURE 1. DGS CSRR (Design A). (a) top and (b) bottom.

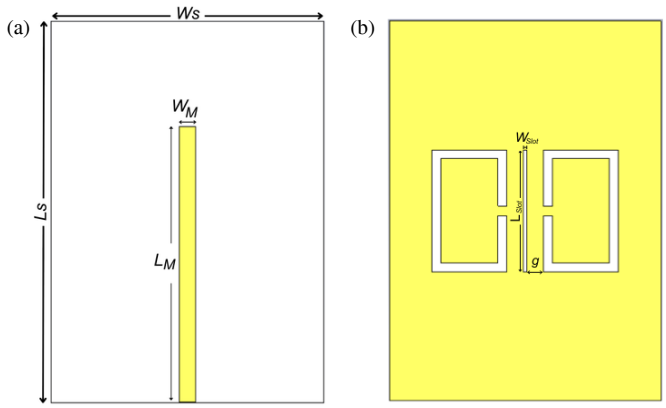

FIGURE 2. DGS CSRR with added slot (Design B). (a) top and (b) bottom.

design are simplifying circuit design by reducing connections and components, thus potentially enhancing efficiency and reliabilities. Its compact nature enables seamless integration into miniaturized and embedded applications, optimizing space and power use in constrained environments.

Several recent studies have explored the use of DGS and CSRR structures in microwave sensors. For instance, [36] presented a sensor with a double-ring CSRR and DGS for detecting ammoniacal nitrogen in water, achieving a Q-factor of 120. The use of DGS helped improve electric field concentration and sensor response. In another study [37], a dual-band sensor based on CSRRs etched into the ground plane showed strong field confinement and a high Q-factor of 267.5, useful for measuring dielectric substrates. A third design [38] used a dumbbell-shaped DGS with a microstrip line and series gap to measure humidity. This sensor achieved a Q-factor of 138 and demonstrated improved sensitivity by combining resonance and antiresonance behavior. These examples show how different ground plane modifications affect performance. However, most of these sensors are two-port and focused on liquids or gases. In comparison, the current work uses a single-port DGS-CSRR structure designed for solid materials. This design helps reduce complexity and shows higher Q-factors and good sensitivity, making it suitable for compact and efficient solid material sensing.

Therefore, this paper proposes a single-port DGS CSRR sensor, a simple microwave sensor optimized for high-Q operation and enhanced sensitivity in solid material characterization within the permittivity (dielectric constant) ranging from 1 to 10. The study examines two single-port microwave sensor configurations: one based on DGS CSRR (Design A) and the other incorporating a DGS CSRR with an added slot (Design B), both operating in the 1.5–3 GHz frequency range.

2. METHODOLOGY

2.1. Sensor Design and Equivalent Circuit

The proposed single-port microwave sensor is developed using planar microstrip technology integrated with a DGS and CSRR for solid material characterization. The sensor designs are based on a Rogers RT/duroid 5880 substrate with a dielectric constant of 2.2 and a thickness of 0.787 mm. It was designed to operate within the 1.5–3.0 GHz frequency range, with a target resonance frequency of 2.4 GHz, which lies within the Industrial Scientific and Medical (ISM) band [39], making it suitable for industrial and scientific applications. The sensor dimensions are compact, measuring 40 mm $\times$ 56 mm, allowing ease of fabrication and integration into measurement setups. Two configurations of the sensor are studied. The first incorporates a DGS with CSSR structure (Design A) beneath the ground plane to enhance field confinement and produces a high Q-factor. The second configuration builds upon it by introducing an additional slot in the ground plane (Design B), further strengthening the electromagnetic coupling and sharpening the resonance characteristics. These design variations are intended to evaluate the effect of ground plane modification on the sensor's Q-factor and sensitivity.

The physical layout and structural details of the proposed microwave sensor designs are shown in Figure 1 and Figure 2, illustrating the top and bottom views of the sensor configurations. These designs are based on microstrip technology (on the top layer) with integrated DGS CSRR (on the bottom layer) to enhance electromagnetic field interaction. The corresponding design parameters, including dimensions of the resonator and ground plane structures, are listed in Table 1. These dimensions were finalized in simulation and selected to ensure compact size, effective resonance behavior, and sensitivity at the targeted frequency range for material characterizations.

TABLE 1. Design dimensions.

Parameter	Value	Parameter	Value
(L_S)	56 mm	(W)	11 mm
(W_S)	40 mm	(g_{DGS})	1.4 mm
(h)	0.787 mm	(g_{Ring})	5.4 mm
(c)	17.5 µm	(L_{Slot})	18 mm
(L_M)	40.45 mm	(W_{Slot})	0.5 mm
(W_M)	2.44 mm	(g)	2.45 mm
(L)	18 mm	(I_w)	1.3 mm

2.2. Equivalent Circuit

The equivalent circuit model of the proposed sensor design is shown in Figure 3, representing the electrical behavior of the microstrip transmission line integrated with a defected ground structure in LC circuit representation. The model includes a series inductance $L_{T_{Line}}$ and a shunt capacitance $C_{T_{Line}}$, which reflect the characteristics of the transmission path and the substrate. The DGS is modeled using a parallel combination of inductance L_{DGS} and capacitance C_{DGS}, connected beneath the signal line. A coupling capacitance C_S is also included to represent the interaction between the signal line and ground plane. Figure 4 compares the simulated S-parameters of the equivalent circuit with those of the electromagnetic (EM) simulation, with the equivalent circuit simulation showing a poor Q-factor that has been optimized in the EM simulation for Designs A and B. The extracted component values used in the circuit model are listed in Table 2. This configuration captures the sensor's resonant response, highlighting how the DGS enhances field concentration and improves sensitivity [31, 33]. The model serves as a useful reference for predicting shifts in resonance caused by variations in the dielectric properties of the material under test, supporting both simulation and experimental validation.

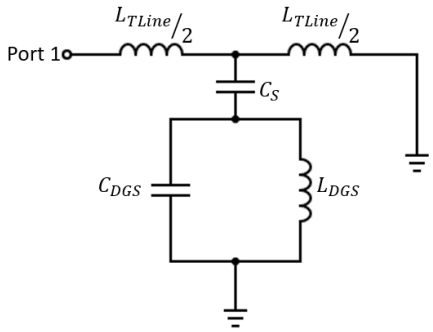

FIGURE 3. Equivalent circuit of the DGS CSRR sensor designs [31].

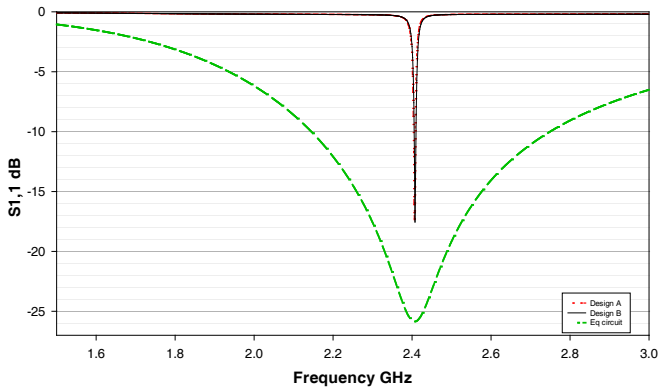

FIGURE 4. Simulated equivalent circuit versus sensor designs.

2.3. Q-Factor and Sensitivity

Quality factor (Q-factor) is a key parameter in the evaluation of resonant structures, as it directly affects the accuracy and resolution of sensing applications, particularly when comparing simulated and measured data. A higher Q-factor enhances the sensor's capability to detect subtle variations in the properties

TABLE 2. Equivalent circuit parameters.

Parameter	Value
L_{TLine}	9.24 nH
C_S	0.43 nF
L_{DGS}	4.2 nH
C_{DGS}	0.61 nF

of the material under test. For the sensor described in this study, the Q-factor is determined using the following relationship:

$$Q_f = \frac{2f_o}{BW_{-3\text{dB}}} \tag{1}$$

where f_o is the resonant frequency of the unloaded sensor, and $BW_{-3\,\text{dB}}$ is the bandwidth measured at the -3 dB return loss level.

Sensor sensitivity is also essential and is directly influenced by the dielectric constant of the material under test. When the material under test (MUT) is placed in the region of maximum electric field strength, particularly in the enhanced field zones created by the defected ground structure, the sensor experiences a shift in resonant frequency [21]. This shift provides the basis for evaluating how sensitively the sensor responds to changes in permittivity. The sensitivity (S) is calculated as the relative frequency shift, normalized to the dielectric constant of the MUT. According to [21, 40], the sensitivity of the proposed sensor can be expressed as:

$$S = \frac{|f_{MUT} - f_o|}{f_o} \times \left(\frac{1}{\varepsilon_{MUT} - 1}\right) \times 100\% \tag{2}$$

Here, f_{MUT} denotes the resonant frequency when the MUT is present, and ε_{MUT} is the dielectric constant of the MUT. This formulation helps quantify how sensitively the sensor responds to material changes, supporting its use in precise dielectric characterization.

2.4. Fabrication and Measurement Procedures

The sensor prototypes were fabricated using UV lithography and chemical etching. The design was exported as a 2D DXF file, printed on matte film, and laminated onto a substrate. UV exposure imprinted the layout, followed by washing and ferric chloride etching to remove unwanted copper. Finally, the substrates were cleaned, dried, and fitted with SMA connectors.

The sensor measurement setup is shown in Figure 5. This setup uses a Vector Network Analyzer (VNA) to measure dielectric properties by analyzing the return loss (S_{11}) shifts with different materials placed on the sensors. Meanwhile, Figure 6 displays the fabricated sensors' top and ground plane layouts (Designs A and B).

For performance evaluation, measurements were performed using a calibrated VNA. The initial step involved capturing the unloaded S_{11} response to determine the baseline resonant frequency. Subsequently, material under test (MUT) was positioned in the area of maximum electric field strength as identified in the simulation process. The VNA recorded the resulting

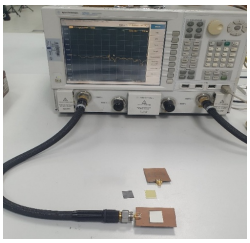

FIGURE 5. Measurements setup.

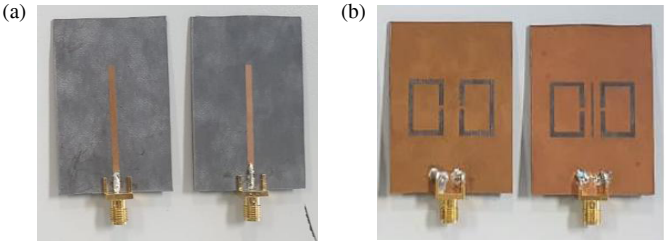

FIGURE 6. Fabricated sensors. (a) Top view of and (b) bottom view.

frequency shifts, which were used to assess the sensor's sensitivity.

3. RESULTS AND DISCUSSION

3.1. Design Performance and Analysis

The electric field (E-field) distribution is first simulated to identify the optimal sensing region of the proposed sensor. As shown in Figure 7, the highest E-field intensity is found on the DGS SRR structure for both designs, indicating the most responsive area for placing the MUT. This region was used in both simulations and measurements to ensure accurate detection of dielectric changes. The difference in field magnitude between the two designs is due to the slot in Design B, which spreads the field over a wider area. Design A, without the slot, has a higher field concentration at a single point, resulting in a peak value of 1.63×10^5 V/m. In contrast, Design B has a lower peak of 1.28×10^5 V/m because the slot redistributes the field. Although the peak is lower, this spreading improves the interaction with the MUT and contributes to better sensing performance.

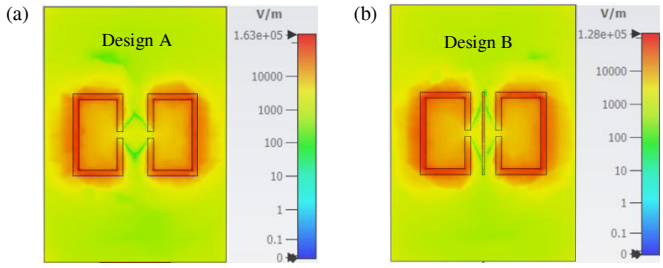

FIGURE 7. E-field distribution of the proposed sensors. (a) Design A and (b) Design B.

The resonance responses of Designs A and B are illustrated in Figure 8 and Figure 9, respectively. The DGS CSRR sensor without a slot (Design A) demonstrated a simulated resonant frequency of 2.406 GHz and a measured frequency of 2.476 GHz, corresponding to a frequency shift of 70 MHz. It achieved a return loss of -17.36 dB in simulation and -7.09 dB in measurement, resulting in a return loss drop rate of 59 percent. The Q-factor was calculated to be 332, indicating stable resonance and effective coupling performance.

In contrast, the DGS CSRR sensor with a slot (Design B) showed enhanced Q-factor performance. The simulated and measured resonant frequencies were 2.408 and 2.487 GHz, respectively, with a slightly larger frequency shift of 79 MHz. Return loss values were -17.54 dB in simulation and -6.65 dB in measurement, with a return loss drop rate of 62 percent. This design achieved a higher Q-factor of 357, reflecting improved resonance sharpness and expected for better sensitivity.

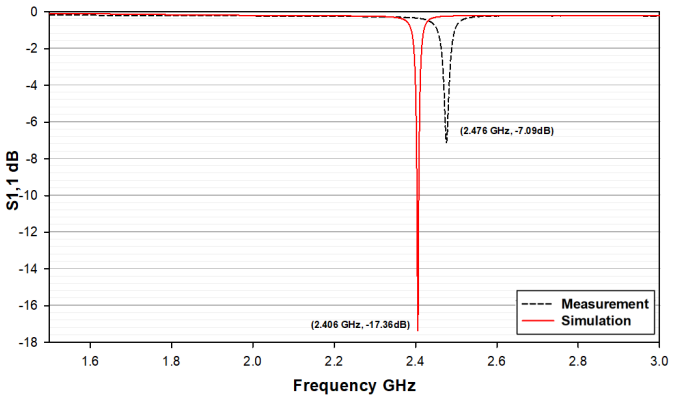

FIGURE 8. Simulation verses measurement of Design A.

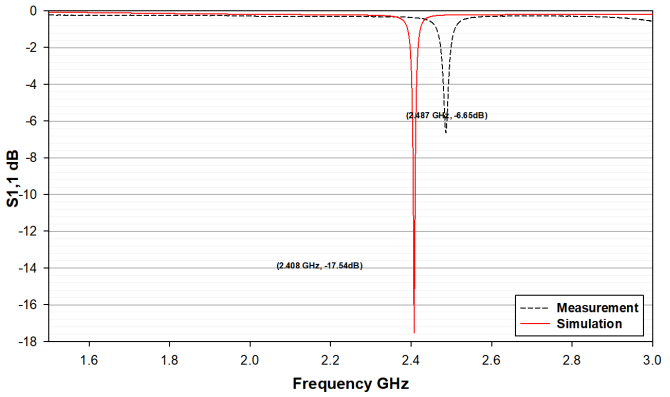

FIGURE 9. Simulation versus measurement of Design B.

Summary performance metrics, including resonant frequency, return loss, frequency shift, and Q-factor, are provided in Table 3 for direct comparison. The results confirm that introducing a slot into the DGS CSRR improved the sensor's Q-factor. The slot contributes to stronger electromagnetic coupling and better impedance control, leading to higher Q-factor.

The differences observed between the simulated and measured return loss values can be attributed to several practical factors. They include copper surface roughness, imperfect soldering of the SMA connectors, and minor dimensional devi-

TABLE 3. Comparison of the proposed sensors (simulation and measurement).

Parameter	DGS CSRR (Design A)	DGS CSRR with Slot (Design B)
Resonant Frequency (simulation)	2.406 GHz	2.408 GHz
Resonant Frequency (measurement)	2.476 GHz	2.487 GHz
Return Loss (simulation)	−17.36 dB	−17.54 dB
Return Loss (measurement)	−7.09 dB	−6.65 dB
Q-factor (simulation)	332	357

ations during fabrication. For example, dimensional deviations of ± 0.1 mm in the resonator gap or trace width, which are common during chemical etching, can influence the resonance characteristics. Additionally, the dielectric constant of the RO5880 substrate has a specified tolerance of 2.20 ± 0.02, and such variation can cause measurable shifts in resonant frequency and contribute to return loss discrepancies between simulation and measurement. Although the simulated return losses are higher than the measured ones, the resonance frequencies remain closely aligned. The slight deviation between the simulated and measured results can be attributed to fabrication tolerances, material imperfections, and measurement setup inconsistencies. Despite these variations, the sensor demonstrates strong resonance characteristics and adequate sensitivity, confirming the reliability of the design and its suitability for dielectric characterization applications.

Then, based on the simulated design performance, the well-known polynomial fitting curve is plotted to show the relationship between permittivity and resonance frequency. A second-order polynomial equation is derived based on the tested resonance point used because it provides a simple and accurate way to represent this relationship by [21, 41, 42]. This method is implemented to measure the dielectric constant of materials based on their resonance frequency. The equation is expressed as:

$$\varepsilon_r = af_o^2 + bf_o + c \tag{3}$$

where f_0 represents the shifted resonant frequency, while a, b, and c are coefficients.

Figures 10(a) and (b) show the simulated polynomial fitting curve for resonant frequency versus permittivity for Design A and Design B, respectively. A significant frequency shift can be observed in the resonance point for different permittivity values of any material between 1 to 10. This affirms that the capability of high sensitivity on the proposed DGS CSRR sensors for solid material characterizations.

The regression equations extracted from the plots can be expressed for Design A and Design B, respectively, as follows:

$$\varepsilon_r = 18.813f_o^2 - 101.32f_o + 135.71 \tag{4}$$

$$\varepsilon_r = 20.535f_o^2 - 105.35f_o + 135.49 \tag{5}$$

3.2. Analysis of the Proposed DGS-CSRR Sensors with Solid Materials

Design A was tested with multiple materials under test (MUT), including air, RT Duroid 5880, RO4350, and FR-4, corresponding to dielectric constants of 1.0, 2.2, 3.48, and 4.4, respectively. The sensor's response, shown in Figure 11 for simulation and Figure 12 for measurement, demonstrates clear shifts in resonant frequency and return loss as the permittivity (dielectric constant) of the MUT increases. The results would confirm the sensor's sensitivity to dielectric variations.

In the simulated results, the resonant frequency decreased from 2.409 GHz for air to 2.124 GHz for FR-4, while return loss ranged from −18.2 dB to −20.26 dB. The Q-factor improved from 311 to 365, indicating sharper resonance at higher permittivity levels. Measured data showed similar trends, with frequencies shifting from 2.476 to 2.32 GHz across the same materials. Return loss values ranged between −7.11 dB and −4.3 dB, with Q-factors increasing from 275 to 329. These differences between simulated and measured results are likely due to fabrication tolerances and environmental conditions during measurement. A summary of all parameters is provided in Table 4.

Meanwhile, Design B was evaluated using the same MUTs. As shown in Figure 13 (simulation) and Figure 14 (measurement), the sensor demonstrated consistent shifts in resonant frequency and return loss in response to changes in material permittivity, confirming its effectiveness in dielectric characterization. Table 5 shows the comparison between simulation and measurement with MUT for Design B.

3.3. Sensor's Sensitivity Analysis

The sensor's sensitivity to variations in dielectric constant was evaluated using RO5880, RO4350, and FR-4. As shown in Table 6, higher permittivity values produced larger resonant frequency shifts, confirming the sensor's effectiveness in solid material characterization. Design B consistently showed greater sensitivity than Design A. For example, sensitivity for RO5880 increased from 2.13 to 4.71 with the addition of the slot (Design B). Similar sensitivity improvements were observed

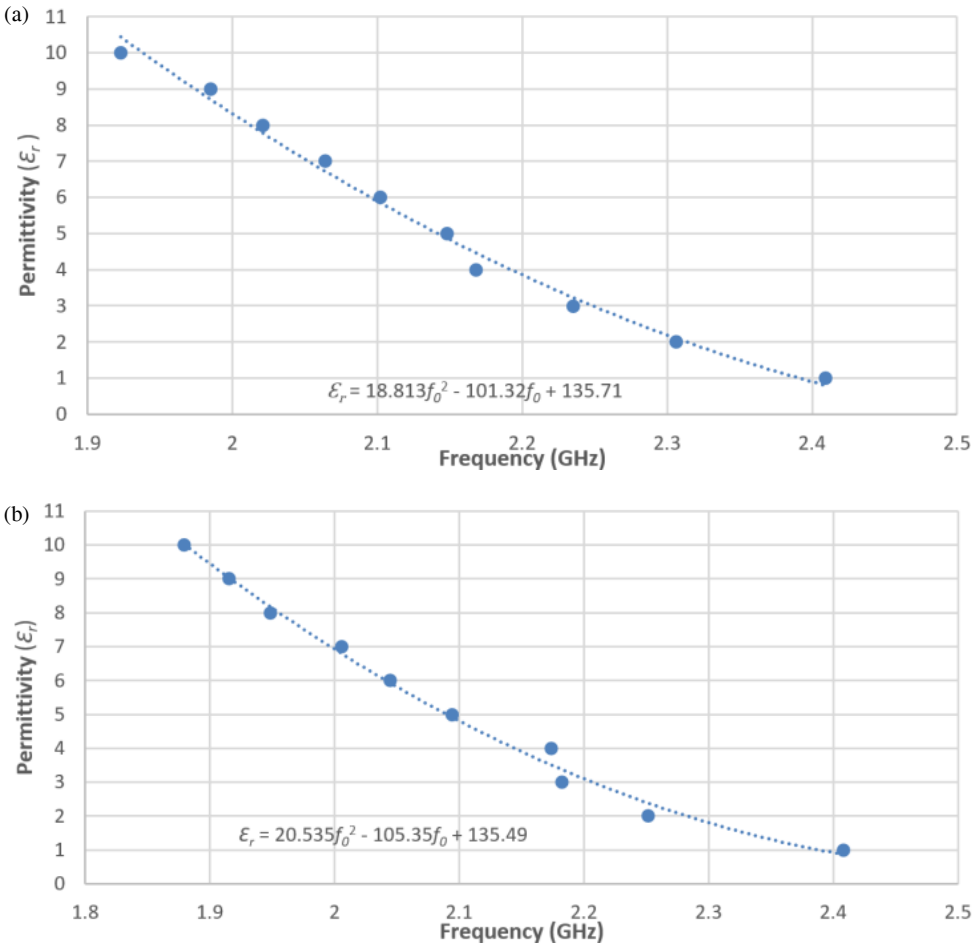

FIGURE 10. Simulated polynomial fitting curve for resonant frequency versus permittivity for (a) Design A and (b) Design B.

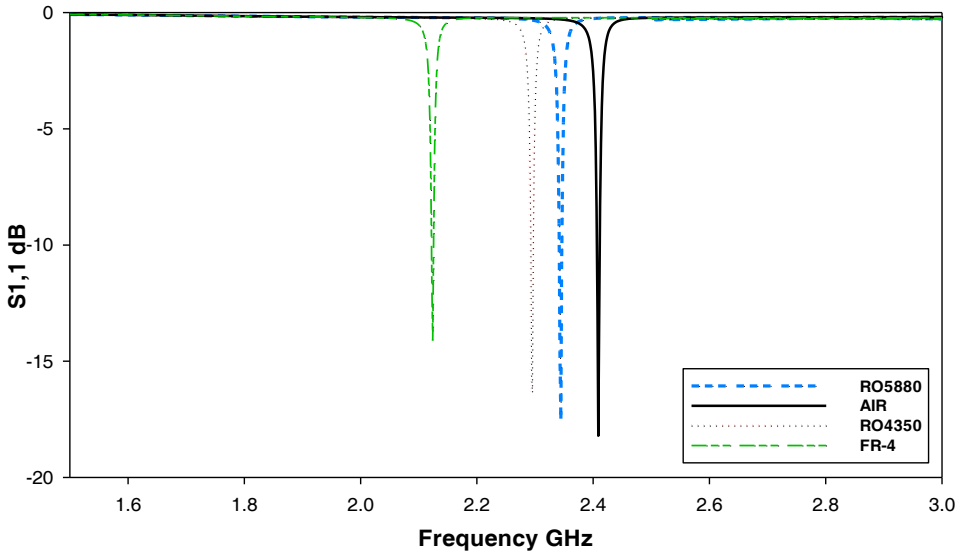

FIGURE 11. Simulation of the S_{11} of Design A with MUT.

for RO4350 and FR-4. This enhancement is attributed to improved field concentration and stronger interaction between the DGS CSRR sensor and the material under test (MUT), making the slotted configuration (Design B) more suitable for applications requiring high detection accuracy.

The results show that the proposed DGS CSRR sensors are responsive to changes in the dielectric properties of solid mate-

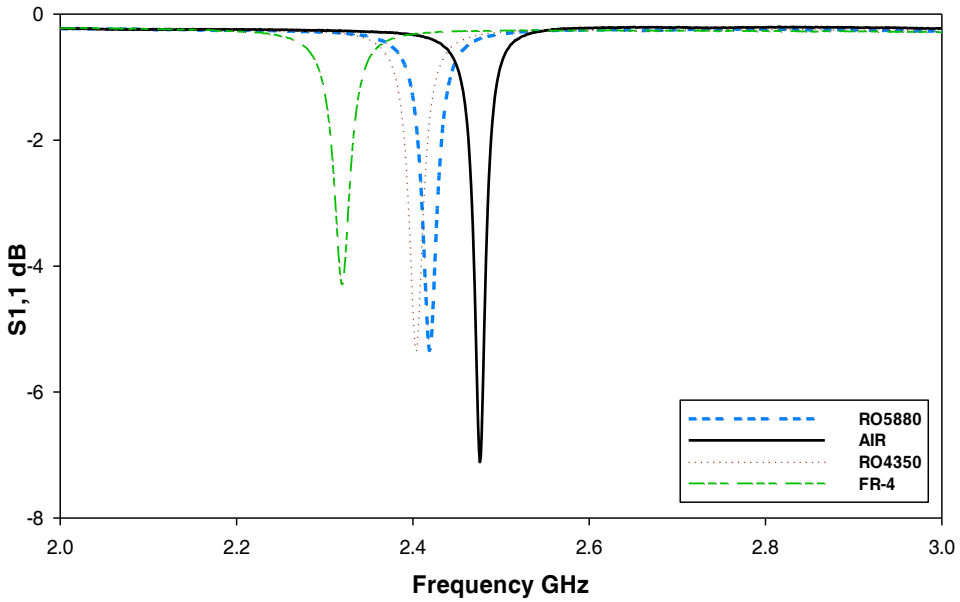

FIGURE 12. Measurement of the S_{11} of Design A with MUT.

TABLE 4. Comparison of simulation and measurement with MUT for Design A.

Parameter \ MUT	Air	RO5880	RO4350	FR4
Resonant Frequency (simulation)	2.409 GHz	2.345 GHz	2.295 GHz	2.124 GHz
Resonant Frequency (measurement)	2.476 GHz	2.419 GHz	2.403 GHz	2.32 GHz
Return Loss (S_{11}) (simulation)	−18.2 dB	−17.51 dB	−16.35 dB	−14.11 dB
Return Loss (S_{11}) (measurement)	−7.11 dB	−5.34 dB	−5.33 dB	−4.3 dB
Q-factor (simulation)	311	322	334	365
Q-factor (measurement)	275	285	283	329

TABLE 5. Comparison of simulation and measurement with MUT for Design B.

Parameter \ MUT	Air	RO5880	RO4350	FR4
Resonant Frequency (simulation)	2.342 GHz	2.273 GHz	2.231 GHz	2.081 GHz
Resonant Frequency (measurement)	2.487 GHz	2.431 GHz	2.416 GHz	2.309 GHz
Return Loss (S_{11}) (simulation)	−19.79 dB	−17.78 dB	−16.61 dB	−15.36 dB
Return Loss (S_{11}) (measurement)	−6.65 dB	−5.69 dB	−5.19 dB	−4.6 dB
Q-factor (simulation)	324	335	342	370
Q-factor (measurement)	293	286	302	289

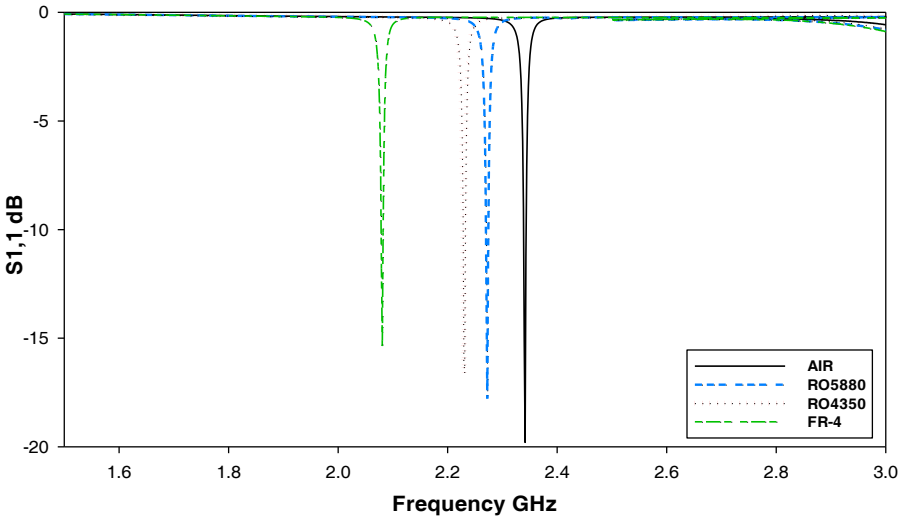

FIGURE 13. Simulation of the S_{11} of Design B with MUT.

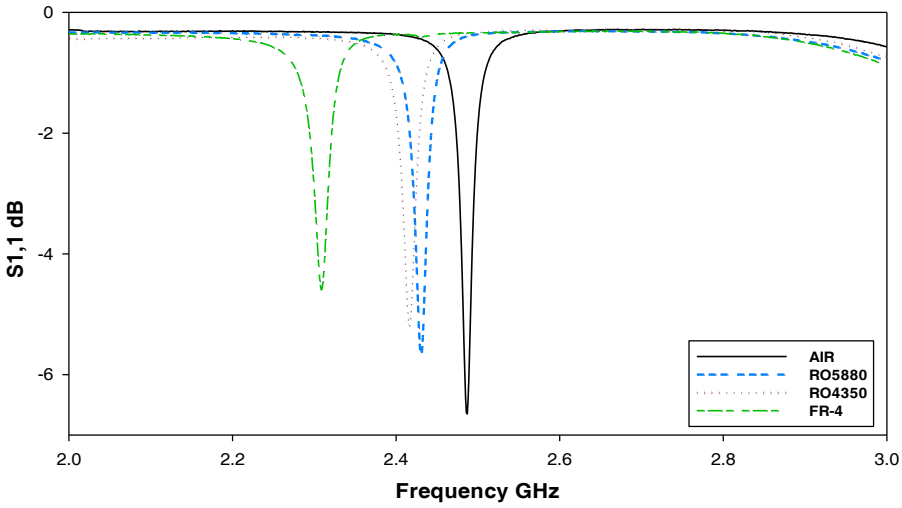

FIGURE 14. Measurement of the S_{11} of Design B with MUT.

TABLE 6. Sensitivity comparison between Design A and Design B.

MUT		RO5880	RO4350	FR-4
ε_{MUT}		2.2	3.48	4.4
f_o (GHz)	Design A	2.406		
	Design B	2.408		
f_{MUT} (GHz)	Design A	2.345	2.295	2.124
	Design B	2.272	2.231	2.081
Sensitivity	Design A	2.11%	1.86%	3.45%
	Design B	4.71%	2.96%	3.99%

rials. Both the Design A and Design B configurations produced consistent resonant frequency shifts, with measurable differences in sensitivity and Q-factor. Design B achieved a higher Q-factor of 357 and greater sensitivity across all tested materials. Simulated and measured trends were generally aligned. However, measured return loss values were lower than simulated results, which is attributed to fabrication-related factors such as surface roughness, etching variations, and imperfect SMA connector soldering. In addition, inconsistencies in positioning the material under test may have reduced coupling efficiency. Despite these limitations, the resonance remained clearly observable, and Q-factor values remained stable, indicating that the sensors perform reliably under practical testing conditions.

3.4. Comparison

Table 7 compares DGS SRR or DGS CSRR configurations based on frequency, Q-factor, and port type (DSRR = double split ring resonator, CDSRR = complementary double split ring resonator, DCSRR = double complementary split ring resonator). Prior research used 2-port designs, but our work introduces a 1-port approach, reducing size and simplifying connections. Both designs operate around 2.4 GHz, with Design B achieving a higher Q-factor (357) due to an added slot. While the highest Q-factor (520) appears in a 2-port DGS SRR at 2.5 GHz, the 1-port system offers simplicity and compactness.

TABLE 7. Comparison with other research works.

Items / References	Structure	f_o (GHz)	Q-Factor	Port
[22]	DGS DSRR	2.3	398	2-Port
[33]	DGS Triple Ring SRR	2.5	520	2-Port
[34]	DGS DSRR	1.72	97.6	2-Port
[35]	DGS CDSRR	3.46	127	2-Port
[36]	DCSRR	1.150	120	2-Port
[43]	DCSRR	2.4	120	2-Port
[44]	DCSRR	3.56	345	2-Port
This work (Design A)	DGS CSRR	2.406	332	1-Port
This work (Design B)	DGS CSRR with added slot	2.408	357	1-Port

This study demonstrates that a 1-port DGS CSRR design enhances performance while optimizing integration in simplified systems.

4. CONCLUSION

Two single-port microwave sensors were designed and fabricated based on DGS CSRR (Design A) and DGS CSRR with an added slot (Design B) for the characterization of solid materials. The proposed sensors were tested using RO5880, RO4350, and FR-4 as the materials under test. Results from both simulation and measurement showed that the sensor with a slot on the DGS CSRR (Design B) exhibited a higher Q-factor of 357 and greater sensitivity than Design A. A clear relationship was observed between the permittivity (dielectric constant) of the tested materials and the corresponding shift in resonant frequency.

ACKNOWLEDGEMENT

The authors would like to acknowledge the Ministry of Higher Education (MOHE) Malaysia for supporting this research under the Fundamental Research Grant Scheme (FRGS), Grant No: FRGS/1/2023/TK07/UTEM/02/18. The authors also thank Universiti Teknikal Malaysia Melaka (UTeM) for the Kesidang Scholarship, and extend their appreciation to the Centre for Research and Innovation Management (CRIM) and the School of Graduate Studies (SPS) at UTeM for their administrative and research support.

REFERENCES

[1] Khalil, M. A., W. H. Yong, T. Batool, A. Hoque, L. Y. Chiong, H. H. Goh, T. A. Kurniawan, M. S. Soliman, and M. T. Islam, "Highly sensitive split ring resonator-based sensor for quality monitoring of edible oils," *Scientific Reports*, Vol. 15, No. 1, 2283, 2025.

[2] Chen, L.-F., C. K. Ong, C. P. Neo, V. V. Varadan, and V. K. Varadan, *Microwave Electronics: Measurement and Materials Characterization*, John Wiley & Sons, 2004.

[3] Waser, R., *Nanoelectronics and Information Technology: Advanced Electronic Materials and Novel Devices*, John Wiley & Sons, 2012.

[4] Alhegazi, A., Z. Zakaria, N. A. Shairi, T. Sutikno, R. A. Alahnomi, and A. I. Abu-Khadrah, "Analysis and investigation of a novel microwave sensor with high Q-factor for oil sensing," *Indonesian Journal of Electrical Engineering and Computer Science*, Vol. 12, No. 3, 1407–1412, 2018.

[5] Alhegazi, A., Z. Zakaria, N. A. Shairi, T. Sutikno, R. A. Alahnomi, and A. I. Abu-Khadrah, "Analysis and investigation of a novel microwave sensor with high Q-factor for liquid characterization," *TELKOMNIKA (Telecommunication Computing Electronics and Control)*, Vol. 17, No. 2, 1065–1070, 2019.

[6] Mayani, M. G., F. J. Herraiz-Martínez, J. M. Domingo, and R. Giannetti, "Resonator-based microwave metamaterial sensors for instrumentation: Survey, classification, and performance comparison," *IEEE Transactions on Instrumentation and Measurement*, Vol. 70, 1–14, 2021.

[7] Huang, T., H. Liu, C. Guo, L. Feng, and L. Geng, "3-D printed mm-Wave filter using increased-height DGS resonator for spurious suppression," *IEEE Transactions on Circuits and Systems II: Express Briefs*, Vol. 69, No. 11, 4293–4297, 2022.

[8] Rao, Y., H. J. Qian, B. Yang, R. Gómez-García, and X. Luo, "Dual-band bandpass filter and filtering power divider with ultra-wide upper stopband using hybrid microstrip/DGS dual-resonance cells," *IEEE Access*, Vol. 8, 23 624–23 637, 2020.

[9] İmeci, S. T., B. Tüetüencüe, F. Bešlija, and L. Herceg, "Microstrip filters based on open stubs and SIR for high frequency and ultra-wideband applications," *Journal of Engineering Research*, Vol. 10, No. 3A, 212–223, 2022.

[10] Li, M., T. Yang, X.-X. Yang, D. Zeng, and Z. Yi, "A defected ground structure for TE and TM coupling reduction of dual-polarized antenna array," *IEEE Antennas and Wireless Propagation Letters*, Vol. 23, No. 9, 2648–2652, 2024.

[11] Madni, A. and W. T. Khan, "Design of a compact 4-element GNSS antenna array with high isolation using a defected ground structure (DGS) and a microwave absorber," *IEEE Open Journal of Antennas and Propagation*, Vol. 4, 779–791, 2023.

[12] Tütüncü, B., H. Torpi, and S. T. İmeci, "Directivity improvement of microstrip antenna by inverse refraction metamaterial," *Journal of Engineering Research*, Vol. 7, No. 4, 2019.

[13] Yasin, F. N. M., N. A. Shairi, A. Othman, H. A. Majid, Z. Zakaria, I. M. Ibrahim, and M. H. Jamaluddin, "High isolation of SPDT PIN diode switch using switchable dumbbell-shaped DGS in millimeter wave 28 GHz band," *Bulletin of Electrical Engineering and Informatics*, Vol. 12, No. 6, 3509–3516, 2023.

[14] Othman, A., H. A. Majid, N. A. Shairi, A. A. Zolkefli, N. Al-Fadhali, Z. Z. Abidin, I. M. Ibrahim, and Z. Zakaria, "Millimeter-wave SPDT Discrete switch design with reconfigurable circle loaded dumbbell DGS," in *2022 International Workshop on Antenna Technology (iWAT)*, 49–52, Dublin, Ireland, 2022.

[15] Alngar, O. Z., A. Barakat, and R. K. Pokharel, "High PAE CMOS power amplifier with 44.4% FBW using superimposed dual-band configuration and DGS inductors," *IEEE Microwave and Wireless Components Letters*, Vol. 32, No. 12, 1423–1426, 2022.

[16] Yi, Z. and C. Wang, "Noninvasive glucose sensors using defective-ground-structure coplanar waveguide," *IEEE Sensors Journal*, Vol. 23, No. 1, 195–201, 2023.

[17] Mansour, E., A. Allam, and A. B. Abdel-Rahman, "A novel approach to non-invasive blood glucose sensing based on a defected ground structure," in *2021 15th European Conference on Antennas and Propagation (EuCAP)*, 1–5, Dusseldorf, Germany, 2021.

[18] Muñoz-Enano, J., P. Vélez, M. Gil, and F. Martín, "Frequency-variation sensors for permittivity measurements based on dumbbell-shaped defect ground structures (DB-DGS): Analytical method and sensitivity analysis," *IEEE Sensors Journal*, Vol. 22, No. 10, 9378–9386, 2022.

[19] Li, C., H. Li, L. Wang, X. Fan, Y. Xiong, L. Qian, D. Li, L. Miao, J. Wang, H. Li, and M. Li, "Microwave microfluidic glucose sensor based on a single-port dumbbell defective ground structure," *IEEE Sensors Journal*, Vol. 24, No. 16, 25 670–25 679, 2024.

[20] Hosseinzadeh, S. and M. Yousefi, "A permittivity and conductivity sensor based on microstrip transmission line with defective ground for detection of urea in saline," *IEEE Transactions on Instrumentation and Measurement*, Vol. 73, 1–11, 2024.

[21] Gong, Y., G. Liu, S. Jiang, J. Yu, and T. Qi, "A DGS-CPW microwave sensor loaded with SRR for solid material measurement," *IEEE Transactions on Instrumentation and Measurement*, Vol. 73, 1–8, 2024.

[22] Misran, M. H., M. A. M. Said, M. A. Othman, A. Salleh, S. Suhaimi, and M. Z. Idris, "High sensitivity double split ring resonator-defected ground structure (DSRR-DGS) based microwave sensors for material characterization," in *2024 IEEE Asia-Pacific Conference on Applied Electromagnetics (APACE)*, 440–443, Langkawi, Kedah, Malaysia, 2024.

[23] Choudhary, A. K., S. Barman, T. Moyra, A. Debnath, and A. Bhattacharjee, "Gain enhancement of dual-band microstrip-fed antenna with complementary split ring resonators and rectangular slots embedded in patch for wireless applications using metamaterial cell-based superstrate," in *2021 2nd International Conference on Range Technology (ICORT)*, 1–6, Chandipur, Balasore, India, 2021.

[24] Bahar, A. A. M., Z. Zakaria, A. A. M. Isa, E. Ruslan, and R. A. Alahnomi, "A review of characterization techniques for material's properties measurement using microwave resonant sensor," *Journal of Telecommunication, Electronic and Computer Engineering (JTEC)*, Vol. 7, No. 2, 1–6, 2015.

[25] Tao, S., Y. Gao, B. Li, J. Zhang, M. Qian, and F. Xuan, "Water-based SRR sensor with machine learning algorithms for simultaneous temperature and pressure detection," *IEEE Sensors Journal*, Vol. 25, No. 3, 5470–5477, 2025.

[26] Elsheakh, D. N., E.-H. Mohamed, and A. R. Eldamak, "Blood glucose monitoring biosensor based on multiband split-ring resonator monopole antenna," *Biosensors*, Vol. 15, No. 4, 250, 2025.

[27] Alrayes, N. and M. I. Hussein, "Metamaterial-based sensor design using split ring resonator and Hilbert fractal for biomedical application," *Sensing and Bio-Sensing Research*, Vol. 31, 100395, 2021.

[28] Rusni, I. M., A. Ismail, A. R. H. Alhawari, M. N. Hamidon, and N. A. Yusof, "An aligned-gap and centered-gap rectangular multiple split ring resonator for dielectric sensing applications," *Sensors*, Vol. 14, No. 7, 13 134–13 148, 2014.

[29] Mansour, E., M. I. Ahmed, A. Allam, R. K. Pokharel, and A. B. Abdel-Rahman, "A microwave sensor based on double complementary split-ring resonator using hexagonal configuration for sensing diabetics glucose levels," in *2023 17th European Conference on Antennas and Propagation (EuCAP)*, 1–5, Florence, Italy, 2023.

[30] Gan, H.-Y., W.-S. Zhao, Q. Liu, D.-W. Wang, L. Dong, G. Wang, and W.-Y. Yin, "Differential microwave microfluidic sensor based on microstrip complementary split-ring resonator (MC-SRR) structure," *IEEE Sensors Journal*, Vol. 20, No. 11, 5876–5884, 2020.

[31] Albishi, A. M., M. K. E. Badawe, V. Nayyeri, and O. M. Ramahi, "Enhancing the sensitivity of dielectric sensors with multiple coupled complementary split-ring resonators," *IEEE Transactions on Microwave Theory and Techniques*, Vol. 68, No. 10, 4340–4347, 2020.

[32] Alahnomi, R. A., Z. Zakaria, E. Ruslan, S. R. A. Rashid, and A. A. M. Bahar, "High-Q sensor based on symmetrical split ring resonator with spurlines for solids material detection," *IEEE Sensors Journal*, Vol. 17, No. 9, 2766–2775, 2017.

[33] Al-Gburi, A. J. A., N. A. Rahman, Z. Zakaria, and M. Palandoken, "Detection of semi-solid materials utilizing triple-rings CSRR microwave sensor," *Sensors*, Vol. 23, No. 6, 3058, 2023.

[34] Ye, W., D.-W. Wang, J. Wang, G. Wang, and W.-S. Zhao, "An improved split-ring resonator-based sensor for microfluidic applications," *Sensors*, Vol. 22, No. 21, 8534, 2022.

[35] Ikhsan, F. H., Y. S. Khee, S. H. Dahlan, F. Esa, and V. Nayyeri, "Synthesis and characterization of polymer (PDMS-FE3O4) Magneto-dielectric material based on complementary double split ring resonator," *Progress In Electromagnetics Research C*, Vol. 141, 79–87, 2024.

[36] Samsuri, W. N. W. M., M. F. Sapuri, S. A. E. A. Rahim, F. A. M. Kasran, N. Yusof, and Z. I. Khan, "High Q double-ring complementary split ring resonator to detect ammoniacal nitrogen for water quality applications," in *2023 IEEE Symposium on Wireless Technology & Applications (ISWTA)*, 174–178, Kuala Lumpur, Malaysia, Aug. 2023.

[37] Armghan, A., T. M. Alanazi, A. Altaf, and T. Haq, "Characterization of dielectric substrates using dual band microwave sensor," *IEEE Access*, Vol. 9, 62 779–62 787, 2021.

[38] Kurniawati, N., P. Vélez, P. Casacuberta, L. Su, X. Canalias, and F. Martín, "Microstrip line loaded with series gap and dumbbell defect-ground-structure (DB-DGS) resonator for highly sensitive sensing based on resonance/antiresonance: Application to humidity measurements," *IEEE Sensors Letters*, Vol. 9, No. 6, 1–4, 2025.

[39] Ruiz-Garcia, L., L. Lunadei, P. Barreiro, and J. I. Robla, "A review of wireless sensor technologies and applications in agriculture and food industry: State of the art and current trends," *Sensors*, Vol. 9, No. 6, 4728–4750, 2009.

[40] Zhang, J., G. Liu, S. Jiang, Y. Gong, and R. Zhang, "A microwave sensor based on grounded coplanar waveguide for solid material measurement," *IEEE Sensors Journal*, Vol. 25, No. 3,

4192–4200, 2024.

[41] Jang, S.-Y. and J.-R. Yang, "Double split-ring resonator for dielectric constant measurement of solids and liquids," *Journal of Electromagnetic Engineering and Science*, Vol. 22, No. 2, 122–128, 2022.

[42] Alam, S., Z. Zakaria, I. Surjati, N. A. Shairi, M. Alaydrus, and T. Firmansyah, "Integrated microwave sensor and antenna sensor based on dual T-shaped resonator structures for contact and noncontact characterization of solid material," *IEEE Sensors Journal*, Vol. 23, No. 12, 13 010–13 018, 2023.

[43] Buragohain, A., A. T. T. Mostako, and G. S. Das, "Low-cost CSRR based sensor for determination of dielectric constant of liquid samples," *IEEE Sensors Journal*, Vol. 21, No. 24, 27 450–27 457, 2021.

[44] Alsaif, H., M. R. Islam, A. Hoque, M. S. Soliman, M. S. Islam, and M. T. Islam, "Dual circular complementary split ring resonator based metamaterial sensor with high sensitivity and quality factor for textile material detection," *APL Materials*, Vol. 12, No. 3, 031136, 2024.